Water adsorption and dissociation on $SrTiO_3$(001) revisited: A density functional theory study

Hannes Guhl,[1,2] Wolfram Miller,[2] and Karsten Reuter[1,3]
[1]*Fritz-Haber-Institut der Max-Planck-Gesellschaft, Faradayweg 4-6, D-14195 Berlin, Germany*
[2]*Leibniz Institute for Crystal Growth (IKZ), Max-Born-Str. 2, D-12489 Berlin, Germany*
[3]*Department Chemie, Technische Universität München, Lichtenbergstr. 4, D-85747 Garching, Germany*
(Received 24 February 2010; revised manuscript received 1 April 2010; published 28 April 2010)

We present a comprehensive density functional theory study addressing the adsorption, dissociation, and successive diffusion of water molecules on the two regular terminations of $SrTiO_3$(001). Combining the obtained supercell-geometry converged energetics within a first-principles thermodynamics framework we are able to reproduce the experimentally observed hydroxylation of the SrO-termination already at lowest background humidity, whereas the TiO_2-termination stays free of water molecules in the regime of low water partial pressures. This different behavior is traced back to the effortless formation of energetically very favorable hydroxyl-pairs on the prior termination. Contrary to the prevalent understanding our calculations indicate that at low coverages also the less water-affine TiO_2-termination can readily decompose water, with the often described molecular state only stabilized toward higher coverages.

DOI: 10.1103/PhysRevB.81.155455 PACS number(s): 68.43.Fg, 71.15.Mb, 68.47.Gh

I. INTRODUCTION

In many of its applications e.g., as photocatalyst, gas sensor, or growth template $SrTiO_3$ is deliberately or unintentionally exposed to aqueous environments. This has motivated a large number of studies on fundamental aspects of the interaction of water with this particular material.[1] As for many other $SrTiO_3$ properties, they have most of all revealed a sensitive dependence on the detailed surface morphology and therewith preparation procedure. Within the surface science philosophy this shifts the focus to the nominally "ideal" two nonpolar terminations of $SrTiO_3$(001), cf. Fig. 1, aiming to establish firm answers for these well defined references. The picture emerging from corresponding studies is an enhanced reactivity of water with the SrO-termination.[2–5] While this termination seems to hydroxylate readily, weak molecular adsorption appears favored at the TiO_2-termination in humid environments. Primarily due to the difficulties of preparing a perfect $SrTiO_3$(001) surface that exhibits only one defect-free termination, a discomforting degree of uncertainty concerning the adsorption state, structure, and energetics remains. Fortunately, recent experimental works exploiting the chemical sensitivity of a combined atomic force microscopy (AFM) and of the friction force microscopy (FFM) approach have made considerable progress in the surface characterization, being now able not only to identify clearly the two different terminations of the $SrTiO_3$ surface[6,7] but also various adspecies for instance Cu overlayers[8] and nanopatterned organic molecules.[9] A key experiment in this respect is therefore the study by Iwahori *et al.*, which employs these FFM scanning capabilities to explore the adsorption of water separately on TiO_2- and SrO-terminated domains.[10] For a range of water exposures a change in the friction force was only measured above SrO-terminated domains and attributed to surface hydroxylation. This confirms the stronger affinity of water to this domain and sets an upper bound for the water bond strength at the TiO_2 termination.

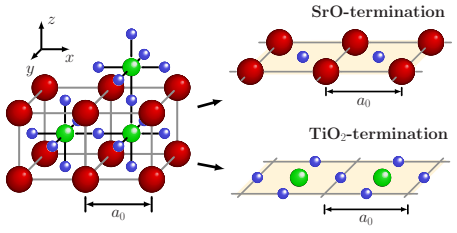

FIG. 1. (Color online) Schematic illustration of the $SrTiO_3$ perovskite bulk structure and the two regular terminations of the (001) surface. Big red (dark) spheres: strontium, big green (bright) spheres: titanium, small blue (bright) spheres: oxygen.

Several theoretical works have already been performed to complement these experimental insights. Wang *et al.* carried out first density functional theory (DFT) calculations with a gradient corrected exchange-correlation (xc) functional and determined a binding energy of molecular water at the TiO_2 termination in somewhat the range indicated by experiment.[11] Unfortunately, the calculations were restricted to small surface unit cells (thereby modeling a high overlayer density), the TiO_2 termination, and did not compare dissociative and molecular adsorption modes. Using a hybrid xc functional Evarestov, Bandura and Alexandrov expanded on the latter two points.[12] However, in their calculations molecular and dissociative adsorption mode were essentially degenerate at the SrO termination and only marginally more stable than molecular water at the TiO_2 termination—thereby questioning the prevalent understanding of a more facile surface hydroxylation of the prior termination. Very recently, Baniecki *et al.* showed that the similar stability at the two terminations is an artifact of the employed small surface unit cells.[13] However, their calculations in larger unit cells did not systematically compare dissociated and molecular adsorption states.

This situation motivates us to revisit the problem with a comprehensive DFT study that systematically addresses the adsorption, dissociation and decomposition of water molecules at both regular $SrTiO_3$(001) terminations. We show that apart from the coverage dependence already identified by Baniecki *et al.* also the employed slab thickness is a hitherto not sufficiently appreciated factor for the binding ener-

getics. The finally obtained converged results are in full agreement with the view deduced from experiment, albeit with a small additional twist: Both terminations are able to dissociate water at low coverage without appreciable barrier. The molecular adsorption state discussed at the TiO_2 termination is only stabilized at higher coverages. At the SrO termination the dissociated water stabilizes in hydroxyl pairs, which we identify as the main factor behind the higher water affinity of this termination observed in the FFM measurements.

II. THEORY

All DFT calculations were performed with the CASTEP (Ref. 14) code using a plane-wave basis together with ultrasoft pseudopotentials[15] as provided in the default library, and the GGA-PBE functional[16] to treat electronic exchange and correlation. Adsorption at the two regular $SrTiO_3(001)$ terminations shown in Fig. 1 was modeled in supercell geometries using mirror-symmetric slabs that zero the internal dipole moment. They are based on the GGA-PBE optimized bulk lattice constant (a_0=3.938 Å), with adsorption at both sides and a vacuum separation exceeding 13 Å. As further detailed below long-range geometric relaxation effects lead to a slow convergence of the binding energetics with slab thickness. We therefore employed up to 13 layer slabs, in which the central three atomic layers were always fixed at their respective bulk positions in the cubic ($Pm\bar{3}m$) perovskite phase, while all other substrate atoms were fully relaxed until the absolute value of all corresponding forces dropped below 0.05 eV/Å.

The central energetic quantity taken from the DFT calculations is the binding energy with respect to gas-phase water defined as

$$E_b = \frac{1}{2}[E_{H_2O \text{ at surf}} - E_{surf} - 2E_{H_2O(gas)}]. \quad (1)$$

Here $E_{H_2O \text{ at surf}}$ is the total energy of the adsorbate covered surface (either with molecular or dissociated water), E_{surf} is the total energy of the clean surface, and $E_{H_2O(gas)}$ is the total energy of the gas-phase H_2O molecule (all three computed at the same plane-wave cutoff). The factor 1/2 accounts for the fact that adsorption is at both sides of the slab and in the sign convention of Eq. (1) a negative value of the binding energy indicates that adsorption is exothermic. The reference energy of the isolated water molecule $E_{H_2O(gas)}$ was calculated in a $(20\times20\times20)$ Å supercell resulting in an optimized OH-bond length of 0.99 Å and a dissociation energy of −2.47 eV as compared to the experimental 0.96 Å and −2.52 eV, respectively.[17] Systematic tests in (1×1) surface unit cells indicate that a cut-off energy for the plane-wave basis set of 430 eV and $(8\times8\times1)$ Monkhorst-Pack (MP) grids[18] for the Brillouin zone integrations ensure a numerical convergence of E_b within ±20 meV. For calculations in larger surface unit cells the MP grids were reduced to maintain the same sampling of reciprocal space.

Energetic barriers and minimum energy paths (MEPs) have been computed using the nudged elastic band (NEB) method[19] in the implementation of the "atomic simulation environment."[20] Corresponding calculations relied on seven atomic layer slabs and (3×3) surface unit cells throughout. The atomic conformations A1–A4 shown in Fig. 4 and B1–B5 in Fig. 7 have first been calculated in individual geometry optimizations. They then served as fixed initial and final states for the ensuing calculation of the connecting MEPs. Systematic tests confirm that neither for the obtained transition nor initial and final state geometries spin polarization plays a role. Furthermore, in all conformations relevant for this work all occupied electronic levels induced by the adsorbed water molecule were located clearly below the valence band maximum, i.e., no artificially delocalized electronic states were encountered that could result from the employed semilocal xc functional and which have for example been clearly demonstrated for the case of hydrogen impurities in bulk TiO_2.[21]

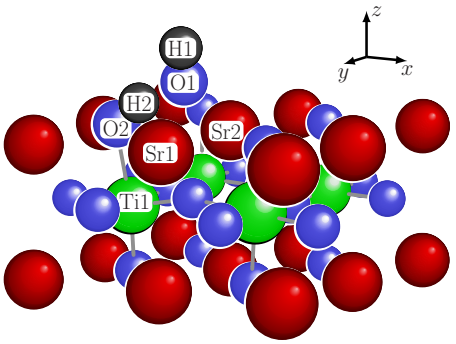

FIG. 2. (Color online) Perspective view of the most favorable adsorption geometry A1 at the SrO termination, in which the water dissociates into an adjacent hydroxyl pair. Atoms discussed in the text and Table I are labeled. Coloring here and in all consecutive figures follows the one of Fig. 1, with small black spheres denoting hydrogen atoms.

III. RESULTS

A. SrO termination

Testing all high-symmetry sites offered by the regular SrO termination we obtain a clear energetic preference for the adsorption geometry A1 displayed in Fig. 2 and further quantified in Table I. In this geometry the water molecule dissociates into two adjacent hydroxyl groups. The O1 and H1 atom from the dissociated water generate a protruding hydroxyl group. Here, the O1 atom sits essentially in a bridge site between two surface strontium cations Sr1 and Sr2, which is the position it would also take in a continuation of the perovskite lattice. The split-off H2 atom of the adsorbing water forms a second hydroxyl group together with a lattice oxygen anion O2. The two hydroxyl groups are strongly tilted toward each other, suggesting the formation of a hydrogen bond that we will further qualify below. Corresponding bonds with a length comparable to the $d_{O1\text{-}H2}$=1.6 Å determined here have recently also been reported for hydroxyl adsorption geometries on alkaline-oxide surfaces.[22]

The hydroxylation lifts the lattice O2 anion quite strongly out of the surface plane. This increases the bond length to the

TABLE I. Selected bond distances in the dissociated adsorption geometry A1 at the SrO-termination, and the molecular B1 and dissociated B2 state at the TiO_2 termination. The labels for the individual atoms are defined in Figs. 2 and 5.

SrO-termination		TiO_2-termination		
	A1 (Å)		B1 (Å)	B2 (Å)
H1-O1	0.97	H1-O1	0.98	0.98
H2-O2	1.01	H2-O2	1.73	0.98
H2-O1	1.60	H2-O1	1.01	2.78
O1-Sr1	2.59	O1-Ti1	2.21	1.84
O1-Sr2	2.55			
O2-Ti1	2.28	Ti1-O3	1.94	2.29

underlying Ti_1 atom by 19%. In turn, the latter reinforces its bond to the underlying third layer O anion with a reduction in the corresponding bond length by 25%. This long range geometric relaxation sequence is the major cause for a slow convergence of the binding energy with the number of slab layers employed in the calculations. As detailed in Table II even for 11 layers slabs there are still remarkable changes of E_b of the order of 50 meV in the larger surface unit-cells. As the geometric relaxations cannot properly develop in the smallest (1×1) cells, there is no such dependence there. On the one hand this reveals how misleading slab-thickness convergence tests in such cells can be, on the other hand it allows us to compare our results to those reported in the earlier studies by Evarestov *et al.*[12] and Baniecki *et al.*,[13] which employed corresponding thin slabs in their calculations restricted to smaller cells. As apparent from Table II (and with equivalent findings compiled in Table III for the TiO_2 termination) the numbers compare all very well, despite the use of a hybrid xc functional in the study by Evarestov *et al.*[12] We take this as confirmation that also the gradient-corrected xc functional employed here is able to capture the essential physics—at a (still) significantly lower computational cost that in turn enables us to perform calculations in much larger surface unit cells. The data for these cells also compiled in Table II on the other hand demonstrates that the latter is a crucial point as the binding energy exhibits a strong coverage dependence, reflecting overall repulsive interactions consistent with the TPD data from Wang *et al.*[3] A value fairly representing the low-coverage limit is only reached in (2×2) cells, and as we will discuss in Sec. III C below, it is this limit that is the appropriate one to discuss the Iwahori FFM experiments.[10]

TABLE II. Binding energies of one water molecule per surface unit cell in the most favorable adsorption state A1 at the SrO termination shown in Fig. 2 and as a function of the number of slab layers N_{slab} employed. Also shown are the values computed by Evarestov *et al.* (Ref. 12) using a hybrid xc functional and by Baniecki *et al.* using a gradient-corrected xc functional similar to the one employed here. All values in eV.

	Surface unit cell		
N_{slab}	(1×1)	(2×2)	(3×3)
	A1	A1	A1
7	−0.83	−1.18	−1.22
9	−0.84	−1.24	−1.30
11	−0.83	−1.28	−1.35
13		−1.31	−1.38
5	−0.79[a]		
7	−0.81[b]	−1.10[b]	

[a]Reference 12.
[b]Reference 13.

At these relevant low coverages the dissociated water state A1 can be reached without any energetic barriers. Figure 3 shows the evolution of the binding energy as a function of the molecule's vertical height above the surface. The barrierless decrease in the binding energy upon approaching the surface is accompanied by a gradual charge transfer to the molecule as reflected by the computed Hirshfeld charges[23] also displayed in Fig. 3. The adsorption process fits therefore perfectly into the picture for dissociative adsorption of water,

TABLE III. Binding energies of one water molecule per surface unit cell in the two most favorable adsorption states at the TiO_2 termination shown in Fig. 5 and as a function of the number of slab layers N_{slab} employed. Also shown are the values computed by Evarestov *et al.* (Ref. 12) using a hybrid xc functional and by Baniecki *et al.* using a semilocal xc functional comparable to the one employed here. All values in eV.

	Surface unit cell					
N_{slab}	(1×1)		(2×2)		(3×3)	
	B1	B2	B1	B2	B1	B2
7	−0.77	−0.58	−0.74	−0.85	−0.71	−0.90
9	−0.78	−0.58	−0.73	−0.92	−0.72	−0.97
11	−0.78	−0.59	−0.73	−0.95	−0.72	−0.99
5	−0.73[a]	−0.64[a]				
7	−0.73[b]		−0.74[b]			

[a]Reference 12.
[b]Reference 13.

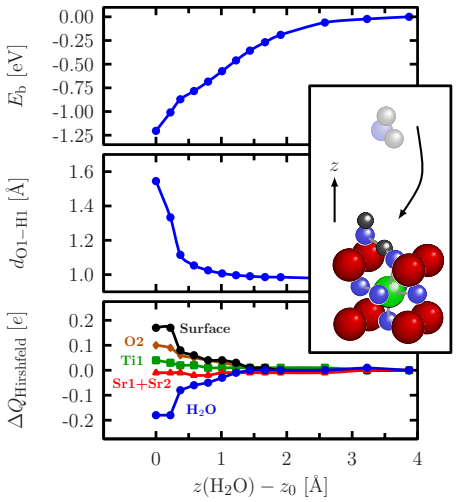

FIG. 3. (Color online) Binding energy, internal O1-H2 bond length and adsorption induced change in the Hirshfeld charges as a function of the vertical height z of the center of mass of an approaching water molecule above the SrO termination. The different atom labels follow the definition given in Fig. 2. The zero reference for the vertical height corresponds to the equilibrium height in the adsorbed state A1. The presented data have been calculated in geometry optimizations, in which the z value of center of mass of the water molecule was constraint at different heights.

with the water as a Lewis acid and the surface, primarily the O2 anion, acting as a Lewis base.[1,17]

While the dissociation into the adjacent hydroxyl pair is thus nonactivated, this is distinctly different for the consecutive decomposition process. Judging from the stability of each hydroxyl group alone, the initially required breaking of the hydroxyl pair will occur via a diffusion hop of the protruding O1-H1 group. Figure 4 shows the computed energy profile for this disintegration pathway. Starting from the most favorable geometry A1 a sizable barrier of ΔE_{A12}=0.93 eV needs to be surmounted. This leads to a shallow metastable geometry A2, in which the O1-H1 group sits in a perovskite-

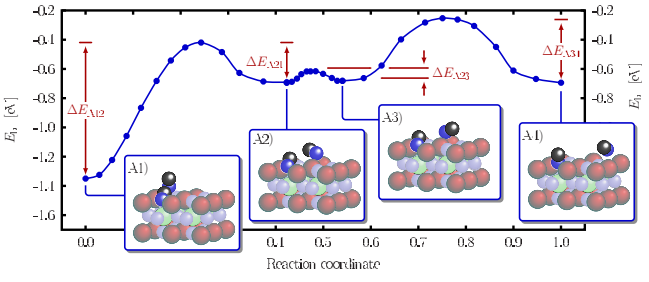

FIG. 4. (Color online) Energy profile for surface diffusion of the protruding O1-H1 hydroxyl group over the SrO-terminated surface. The initial state A1 corresponds to the hydroxyl pair after the immediate water dissociation process shown in Fig. 3. The transition from state A1 to A2 breaks the hydroxyl pair and is accompanied by a substantial energetic barrier. Configurations A2 and A3 differ essentially in the mutual orientation of the two hydroxyl groups, whereas state A4 represents the maximum possible distance of the diffusing species to its original position in a periodically continued (3×3) surface model.

type bridge site one unit cell further away than before. With a computed barrier in excess of 1 eV for consecutive diffusion of the surface H_2 atom, the most favorable pathway for further decomposition proceeds instead through the reorientation of the O1-H1 hydroxyl-group to point away from the original hydroxyl partner. This flip is only connected with a negligibly small barrier ΔE_{A23}=0.08 eV, indicating a very fast dangling dynamics. The ensuing diffusion of the separated O1-H1 hydroxyl-group through hops to adjacent binding sites is then characterized by an intermediate barrier ΔE_{A34}=0.41 eV. Here, we notice that the energetic minima corresponding to the equivalent states A3 and A4 are aligned on the same level. This suggests no further significant long-range interaction between the immobile O1-H1 group and the moving O1-H1 hydroxyl. On the other hand, this energetic level is located 0.67 eV above the one of the initial configuration A1, which thus directly reflects the additional bond strength resulting from the hydroxyl pairing. With such strong attraction between the two hydroxyls generated from the dissociation of one water molecule, the percentage of freely diffusing hydroxyl groups or H atoms resulting from this process will be very small up to very high temperatures.

B. TiO_2 termination

In agreement with the preceding theoretical studies[11–13] we also determine a molecular adsorption state on the TiO_2 termination. The adsorption geometry of this state henceforth denoted B1 is depicted in Fig. 5, with selected bond distances compiled in Table I. Adsorption in this mode induces only small geometric relaxations of the $SrTiO_3$(001) substrate, and accordingly we only observe a weak dependence of the computed binding energy with the number of layers employed in the slab model, cf. Table III. The coverage dependence is equally weak and in contrast to the dissociated state at the SrO termination slightly attractive. We also compute a nonactivated adsorption pathway into this molecular bound state, which is essentially characterized by an increasing charge depletion around the H2 atom to stabilize the O1-Ti1 molecule-surface bond.

As illustrated in Fig. 6 the full separation of the H2 atom to reach a dissociated state B2 is accompanied by a small energy barrier ΔE_{B12}=0.09 eV. In this respect, the molecular state B1 can be considered as a true precursor and its stabilization (in contrast to the SrO termination) fits well to the expectation of a weaker acidity of the Ti cations compared to the Sr cations on $SrTiO_3$(100).[24] In fact, comparing the Hirshfeld-charges in the bottommost panels of Figs. 3 and 7 suggests that the character of the adsorbing water molecule is clearly more basic on the TiO_2-termination with respect to the situation on the SrO termination. On the other hand, at the low coverage corresponding to the (3×3) surface unit-cell calculation behind Fig. 6 the molecular state B1 exhibits only a weakly pronounced metastability, with the ensuing dissociated state B2 (further characterized in Fig. 5 and Table I) more favorable by more than 0.2 eV. Intriguingly and as detailed in Table III, this energetic ordering reverses at higher coverages, with the molecular state B1 more stable in the smallest (1×1) surface unit cell. We

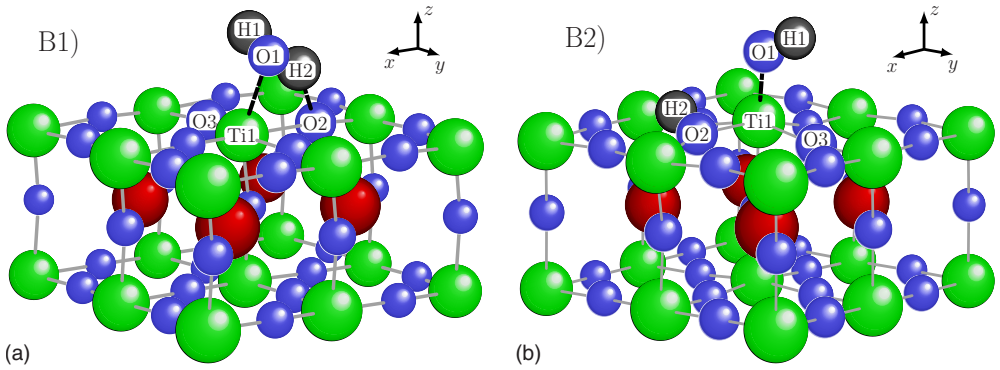

FIG. 5. (Color online) Perspective view of the molecular B1 (left) and dissociated B2 (right) adsorption geometry at the TiO_2 termination. Atoms discussed in the text and Table I are labeled. In a second dissociated state (not shown), which is energetically equivalent to the state B2, the O_1-H_1 group is rotated by 180° degrees and thus points in the same direction as the tilted O2-H2 hydroxyl.

therefore fully reproduce the preference for molecularly adsorbed water obtained in the previous calculations[11–13] but show that this preference is restricted to rather dense packings. In fact, at these coverages one may well imagine an even further increased stability of mixed phases containing both molecular and dissociated water molecules compared to the two pure phases studied here. We did not pursue calculations along this line though as we will demonstrate in the following section that it is the regime of lower coverages that is, e.g., relevant for the Iwahori FFM experiments, and in this low coverage regime dissociation into two surface hydroxyl groups is the preferred adsorption mode with only a slight activation barrier to overcome. We note that these findings are in no contradiction to the frequent interpretation of experimental data exclusively in terms of molecularly adsorbed water.[2–5] Even though an absolute coverage calibration was rarely achieved, it is quite clear that these studies operated mostly in the higher coverage regime. Moreover and as already discussed by Baniecki *et al.*[13] frequently employed fingerprints for "molecular" water [like the appearance of two adsorbate peaks below the O 2*p* valence band in ultraviolet photoemission spectroscopy (UPS) (Refs. 4 and 5)] are not necessarily unambiguous. Indeed, we have verified that the valence states due to the hydroxyl groups in the B2 adsorption mode lie at essentially the same energy as the $3a_1$ molecular orbital of the adsorbed water in the B1 mode, such that even a larger fraction of dissociated water would not easily be distinguished in the UPS spectra.

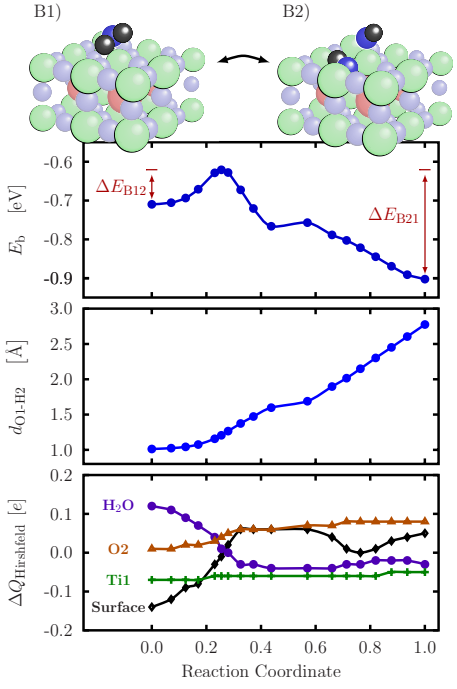

FIG. 6. (Color online) Binding energy, internal O1-H2 bond length and change in the Hirshfeld charges along the reaction pathway from the molecular bound state B1 to the dissociated state B2 at the TiO_2 termination. The different atom labels follow the definition given in Fig. 2. The zero reference for the Hirshfeld charges corresponds to gas-phase water and the clean surface.

In contrast to the SrO termination the preferred mechanism for a further disintegration of the adjacent hydroxyl groups of the dissociated state B2 is not via hopping of the

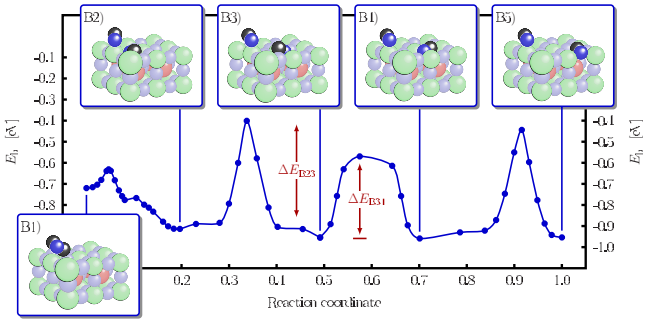

FIG. 7. (Color online) Energy profile for surface diffusion of the split-off H_2 atom over the TiO_2-terminated surface. The initial states B1 and B2 correspond to the molecular precursor and dissociated hydroxyl pair shown in Fig. 5. Further disintegration takes place via a hop of the surface H_2 atom to an adjacent lattice O anion (B3) with a barrier ΔE_{B23}=0.51 eV, followed by a flip of the orientation of the newly formed hydroxyl group toward the neighboring surface unit cell (B4) with a barrier ΔE_{B34}=0.38 eV. With the ensuing equivalent hop exhibiting virtually the same energy profile and suggesting thereby only small longer-range lateral interactions between the hydroxyl groups, the diffusing hydrogen atom H2 has reached in B5 the maximum distance to its original position in B1 that is possible in a periodically continued (3×3)-surface model.

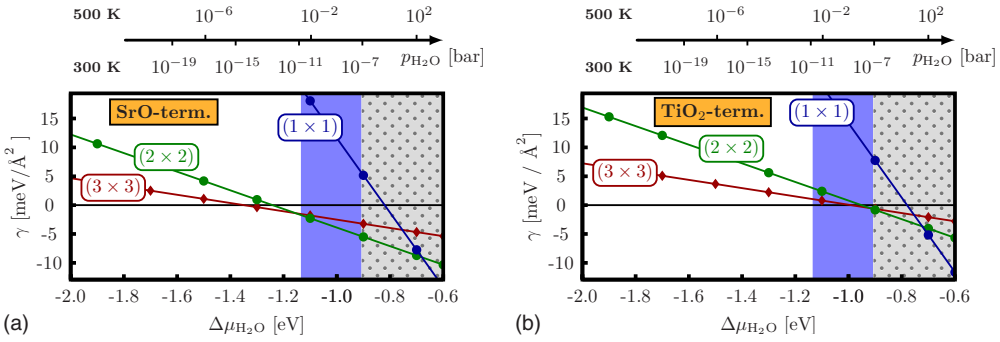

FIG. 8. (Color online) Surface free energies, cf. Eq. (2), of the most stable water adsorption geometries at the different coverages at the SrO-termination (left) and TiO_2 termination (right). In the top x axis, the dependence on the water chemical potential is converted into pressure scales at 300 and 500 K. The plain (blue) background boxes mark the region of gas-phase conditions probed by Iwahori *et al.* in their FFM experiments (Ref. 10), while the dotted (gray) boxes indicate the region above the H_2O-rich limit, i.e., where the present approach assuming equilibrium with water vapor is no longer strictly applicable.

protruding O1-H1 group. We compute a large barrier of 1.5 eV for a corresponding hop to a neighboring Ti cation. Instead, continued diffusion is at this termination much more effective via surface hopping of the split-off H_2 atom. As illustrated in Fig. 7 this mechanism proceeds through a sequence of hops with a barrier of 0.51 eV and reorientation flips with a barrier of 0.38 eV. In the hops the H2 atom breaks the bond to its directly coordinated lattice O partner and jumps to a directly adjacent lattice O anion. In the consecutive flip the thereby formed hydroxyl group changes its tilt direction to the opposite side, therewith enabling another hop to lattice O anions now belonging to a neighboring surface unit cell. Interestingly, the rate-limiting step of 0.51 eV for this diffusion mechanism agrees almost perfectly to the calculated activation barrier for proton diffusion in bulk $SrTiO_3$.[25] A disintegration of the hydroxyls generated through the dissociative adsorption of water is thus not as limiting as at the TiO_2 termination and might actually proceed both through surface and subsurface proton diffusion.

C. First-principles thermodynamics

In order to directly address the Iwahori FFM experiments we now combine the supercell-converged energetics for adsorbed water at the two terminations and at different coverages within a first-principles atomistic thermodynamics framework.[26–30] In this approach we assume the surface to be in equilibrium with a surrounding water vapor environment characterized by a chemical potential μ_{H_2O}. For each surface termination the stable surface structure at a given μ_{H_2O} then minimizes the surface free energy defined as

$$\gamma(\mu_{H_2O}) = \frac{1}{A}[G_{H_2O\ \text{at Surf}} - G_{\text{Surf}} - N_{H_2O}\mu_{H_2O}]. \quad (2)$$

Here, $G_{H_2O\ \text{at Surf}}$ is the Gibbs free energy of the surface covered with N_{H_2O} water molecules per surface area A and G_{Surf} is the Gibbs free energy of the corresponding clean surface. Aiming only for a first assessment we approximate the difference $(G_{H_2O\ \text{at Surf}} - G_{\text{Surf}})$ with the difference of the corresponding total energies, thereby neglecting vibrational free energy and configurational entropy contributions. As discussed in detail in Ref. 30 this is largely justified, as most of these contributions effectively cancel in the difference. A notable exception to this arises from the vibrational free contributions from the adsorbate functional groups, which particularly for hydroxyl or water groups are in general not negligible.[31] We nevertheless omit them here, realizing from the results presented below that the relevant surface terminations to discuss the Iwahori FFM experiments correspond to rather low adsorbate densities.

Contact to the experimental environments can be made by exploiting the relation between chemical potential and gas-phase temperature and pressure. For this we first separate the total energy contribution to the chemical potential

$$\Delta\mu_{H_2O}(T, p_{H_2O}) = \mu_{H_2O}(T, p_{H_2O}) - E_{H_2O(\text{gas})}. \quad (3)$$

At standard pressure $p^\circ_{H_2O} = 1$ bar the relative $\Delta\mu_{H_2O}(T, p^\circ_{H_2O})$ can then be derived from enthalpy H and entropy S differences tabulated in thermochemical tables[32]

$$\Delta\mu_{H_2O}(T, p^\circ_{H_2O}) = [H(T, p^\circ_{H_2O}) - H(0\text{K}, p^\circ_{H_2O})] - T[S(T, p^\circ_{H_2O}) - S(0\text{K}, p^\circ_{H_2O})] \quad (4)$$

From this the relative chemical potential at any other pressure follows finally from the ideal-gas relation

$$\Delta\mu_{H_2O}(T, p_{H_2O}) = \Delta\mu_{H_2O}(T, p^\circ_{H_2O}) + k_B T \ln\left(\frac{p_{H_2O}}{p^\circ_{H_2O}}\right), \quad (5)$$

where k_B is the Boltzmann constant. The latter relation is appropriate as long as the discussion is restricted to humid environments, i.e., those corresponding to the gaseous state of water for any temperature or pressure. This sets an upper bound for $\Delta\mu_{H_2O} = -0.91$ eV, which corresponds to the chemical potential of water at the (experimental) critical point.[31] As we will see in the following the experimental conditions employed in the Iwahori FFM experiments all fall below this H_2O-rich limit.

Figure 8 summarizes the obtained results for the two terminations. Starting the discussion with the SrO termination, the graph shows the surface free energies obtained for the dissociated hydroxyl-pair state A1 at the three coverages cor-

responding to one water molecule per (3×3), (2×2), and (1×1) surface unit cell. Reflecting the absence of significant longer-range lateral interactions between different hydroxyl pairs at the two lower coverages, the corresponding structures become more stable than the clean surface within a narrow chemical potential range. As apparent from Fig. 8 the experimental gas-phase conditions probed in the FFM experiments by Iwahori *et al.*[10] (10^{-11} bar$<p_{H_2O}<10^{-7}$ bar, $T=300$ K) fall clearly above this threshold. The calculations therefore fully support the authors' surmise that the observed increase in the friction-force coefficient on the SrO-terminated domains is due to surface hydroxylation. The observation that the TiO_2 termination stays free of water molecules in the same probed environments is also fully consistent with our calculations. The much smaller binding energy for the dissociated state B2 that is most stable at the lower coverages yields a crossing of the corresponding (3×3) and (2×2) lines with the clean surface reference in Fig. 8 only at chemical potentials toward the upper end of the experimental range. While our calculations thus confirm the interpretation of the FFM data, the consistency demonstrates vice versa that the supercell-converged absolute binding energetics from the employed semilocal xc functional, which stands behind the thermodynamics lines in Fig. 8, is quite reliable. This concurs with the earlier observation that the semilocal energetics agrees closely to the one obtained by Evarestov *et al.* with a hybrid xc functional and reconfirms our assessment that the discrepancies between experiment and theory existing before this work were less due to the treatment of electronic xc but more due to the use of restricted supercell geometries.

At both terminations the dense (1×1) overlayers that were at the focus of the preceding theoretical works become most stable only at a very high chemical potential of $\Delta\mu_{H_2O}\approx-0.7$ eV. This is far outside the relevant conditions for the Iwahori experiments and in fact above the H_2O-rich limit, where the present thermodynamic approach is no longer strictly valid. This said it is nevertheless intriguing to note that recent FFM experiments by Kato *et al.* employed much higher water pressures in excess of 10^{-5} bar at room temperature.[33] They initially observed a loss of the Iwahori friction-force contrast between the two $SrTiO_3(001)$ terminations, which reappeared at a pressure of 10^{-2} bar. The latter threshold corresponds to a $\Delta\mu_{H_2O}=-0.6$ eV, which is only by about 0.1 eV smaller than where our calculations would predict the stabilization of the dense (1×1) overlayers and specifically the hydroxylated A1 phase on the SrO-termination and the molecular B1 phase on the TiO_2 termination. In contrast, for lower chemical potentials down to $\Delta\mu_{H_2O}=-0.77$ eV (corresponding to the lower pressure limit of 10^{-5} bar employed by Kato *et al.*) both terminations would simply be hydroxylated with less dense arrangements. If hydroxylation is indeed the contrast mechanism behind the FFM observations, this would be fully consistent with the interpretation in terms of the formation of a condensed water layer at the threshold pressure of 10^{-2} bar at room temperature proposed by Kato *et al.*[33]

IV. SUMMARY AND CONCLUSIONS

In summary our comprehensive DFT calculations demonstrate that both regular terminations of $SrTiO_3(100)$ are initially able to dissociate water without appreciable barrier. At the SrO termination this leads to stable hydroxyl-pairs in the entire sub-monolayer regime. At the TiO_2 termination a molecular adsorption state is a metastable precursor at low coverages and becomes the most favorable adsorption mode in a dense overlayer. Combining the computed supercell-converged energetics for these adsorption structures within a first-principles atomistic thermodynamics framework we can fully rationalize the friction-force microscopy experiments by Iwahori *et al.*, which indicate a much higher water affinity of the SrO termination. The absolute binding energetics obtained with the semilocal exchange-correlation functional employed in our study is therefore fully consistent with the stringent bounds set by these measurements. The detailed analysis of the continued disintegration of the dissociated water molecules reveals a strong pairing mechanism of the two surface hydroxyls generated from the dissociation of one water molecule at the SrO termination. Rather than the stronger acidity of the Sr cations in $SrTiO_3(001)$ it is the additional stabilization due to this hydroxyl pairing which stands behind the notably different water affinity of the two terminations. A similar pairing mechanism has recently been reported for the alkaline-oxides CaO and BaO (Ref. 22) and we believe this cooperative effect to be an important general feature for low-hydrated oxide surfaces. Another important observation is that the O atom of the protruding hydroxyl group that has formed as a result of the water dissociation process sits in both terminations at the site it would also take in a continuation of the perovskite lattice structure. This is distinctly different to adsorbed O atoms, which we previously found to adsorb in nonperovskite sites.[34] This difference as well as the low mobility of paired hydroxyl groups could be important ingredients toward an atomic-scale understanding of the experimental reports that hydrogen and water increase the growth rate of $SrTiO_3$.[35]

ACKNOWLEDGMENTS

All calculations have been performed on the SGI Altix ICE1-, ICE2-, and XE-computing clusters of the North-German Supercomputing Alliance (HLRN) hosted at the Konrad-Zuse-Zentrum für Informationstechnik in Berlin (ZIB) and at the Regionales Rechenzentrum für Niedersachsen (RRZN) at the Leibniz Universität Hannover. We are particularly grateful to B. Kallies for technical support.

[1] M. A. Henderson, Surf. Sci. Rep. **46**, 1 (2002).
[2] P. A. Cox, R. G. Egdell, and P. D. Naylor, J. Electron Spectrosc. Relat. Phenom. **29**, 247 (1983).
[3] L.-Q. Wang, K. F. Ferris, and G. S. Herman, J. Vac. Sci. Technol. A **20**, 239 (2002).
[4] I. W. Owen, N. B. Brookes, C. H. Richardson, D. R. Warburton, F. M. Quinn, D. Norman, and G. Thornton, Surf. Sci. **178**, 897 (1986).
[5] S. Eriksen, P. D. Naylor, and R. G. Egdell, Spectrochim. Acta, Part A **43**, 1535 (1987).
[6] J. Fompeyrine, R. Berger, H. P. Lang, J. Perret, E. Mächler, Ch. Gerber, and J.-P. Locquet, Appl. Phys. Lett. **72**, 1697 (1998).
[7] K. Iwahori, S. Watanabe, M. Kawai, K. Mizuno, K. Sasaki, and M. Yoshimoto, J. Appl. Phys. **88**, 7099 (2000).
[8] S. Shiraki, M. Nantoh, M. Wakatsuchi, and M. Kawai, J. Appl. Phys. **94**, 3082 (2003).
[9] M. Paradinas, L. Garzón, F. Sánchez, R. Bachelet, D. B. Amabilino, J. Fontcuberta, and C. Ocal, Phys. Chem. Chem. Phys. **12**, 4452 (2010).
[10] K. Iwahori, S. Watanabe, M. Kawai, K. Kobayashi, H. Yamada, and K. Matsushige, J. Appl. Phys. **93**, 3223 (2003).
[11] L.-Q. Wang, K. F. Ferris, S. Azad, and M. H. Engelhard, J. Phys. Chem. B **109**, 4507 (2005).
[12] R. A. Evarestov, A. V. Bandura, and V. E. Alexandrov, Surf. Sci. **601**, 1844 (2007). The numbers cited in Tables II and III include a correction of 0.12 eV for the basis set superposition error as estimated by the authors.
[13] J. D. Baniecki, M. Ishii, K. Kurihara, K. Yamanaka, T. Yano, K. Shinozaki, T. Imada, and Y. Kobayashi, J. Appl. Phys. **106**, 054109 (2009).
[14] S. Clark, M. D. Segall, C. J. Pickard, P. J. Hasnip, M. I. J. Probert, K. Refson, and M. C. Payne, Z. Kristallogr. **220**, 567 (2005).
[15] D. Vanderbilt, Phys. Rev. B **41**, 7892 (1990).
[16] J. P. Perdew, K. Burke, and M. Ernzerhof, Phys. Rev. Lett. **77**, 3865 (1996).
[17] P. A. Thiel and T. E. Madey, Surf. Sci. Rep. **7**, 211 (1987).
[18] H. Monkhorst and J. Pack, Phys. Rev. B **13**, 5188 (1976).
[19] B. P. Henkelman, G. Uberuaga, and H. Jonsson, J. Chem. Phys. **113**, 9901 (2000).
[20] S. R. Bahn and K. W. Jacobsen, Comput. Sci. Eng. **4**, 56 (2002).
[21] E. Finazzi, C. DiValentin, G. Pacchioni, and A. Selloni, J. Chem. Phys. **129**, 154113 (2008).
[22] J. Carrasco, F. Illas, and N. Lopez, Phys. Rev. Lett. **100**, 016101 (2008).
[23] F. L. Hirshfeld, Theor. Chim. Acta **44**, 129 (1977).
[24] T. L. Barr, J. Vac. Sci. Technol. A **9**, 1793 (1991); T. L. Barr and C. R. Brundle, Phys. Rev. B **46**, 9199 (1992).
[25] W. Münch, K.-D. Kreuer, G. Seifertli, and J. Majer, Solid State Ionics **125**, 39 (1999).
[26] C. M. Weinert and M. Scheffler, Mat. Sci. Forum **10-12**, 25 (1986).
[27] M. Scheffler, in *Physics of Solid Surfaces: 1987*, edited by J. Koukal (Elsevier, Amsterdam, 1988); M. Scheffler and J. Dabrowski, Philos. Mag. A **58**, 107 (1988).
[28] E. Kaxiras, Y. Bar-Yam, J. D. Joannopoulos, and K. C. Pandey, Phys. Rev. B **35**, 9625 (1987).
[29] G.-X. Qian, R. M. Martin, and D. J. Chadi, Phys. Rev. B **38**, 7649 (1988).
[30] K. Reuter and M. Scheffler, Phys. Rev. B **65**, 035406 (2001).
[31] Q. Sun, K. Reuter, and M. Scheffler, Phys. Rev. B **67**, 205424 (2003).
[32] D. R. Stull and H. Prophet, *JANAF Thermochemical Tables*, 2nd ed. (U.S. National Bureau of Standards, Washington, D.C., 1971).
[33] H. S. Kato, S. Shiraki, M. Nantoh, and M. Kawai, Surf. Sci. **544**, L722 (2003).
[34] H. Guhl, W. Miller, and K. Reuter, Surf. Sci. **604**, 372 (2010).
[35] T. W. Simpson, J. C. Mitchell, I. V. McCallum, and L. A. Boatner, J. Appl. Phys. **76**, 2711 (1994).